AIP | Journal of Applied Physics

Fabrication of poly(methyl methacrylate)-MoS2/graphene heterostructure for memory device application

Sachin M. Shinde, Golap Kalita, and Masaki Tanemura

Citation: Journal of Applied Physics **116**, 214306 (2014); doi: 10.1063/1.4903552
View online: http://dx.doi.org/10.1063/1.4903552
View Table of Contents: http://scitation.aip.org/content/aip/journal/jap/116/21?ver=pdfcov
Published by the AIP Publishing

Fabrication of poly(methyl methacrylate)-MoS_2/graphene heterostructure for memory device application

Sachin M. Shinde,[1] Golap Kalita,[1,2,a)] and Masaki Tanemura[1]
[1]*Department of Frontier Materials, Nagoya Institute of Technology, Gokiso-cho, Showa-ku, Nagoya 466-8555, Japan*
[2]*Center for Fostering Young and Innovative Researchers, Nagoya Institute of Technology, Gokiso-cho, Showa-ku, Nagoya 466-8555, Japan*

(Received 21 September 2014; accepted 24 November 2014; published online 5 December 2014)

Combination of two dimensional graphene and semi-conducting molybdenum disulfide (MoS_2) is of great interest for various electronic device applications. Here, we demonstrate fabrication of a hybridized structure with the chemical vapor deposited graphene and MoS_2 crystals to configure a memory device. Elongated hexagonal and rhombus shaped MoS_2 crystals are synthesized by sulfurization of thermally evaporated molybdenum oxide (MoO_3) thin film. Scanning transmission electron microscope studies reveal atomic level structure of the synthesized high quality MoS_2 crystals. In the prospect of a memory device fabrication, poly(methyl methacrylate) (PMMA) is used as an insulating dielectric material as well as a supporting layer to transfer the MoS_2 crystals. In the fabricated device, PMMA-MoS_2 and graphene layers act as the functional and electrode materials, respectively. Distinctive bistable electrical switching and nonvolatile rewritable memory effect is observed in the fabricated PMMA-MoS_2/graphene heterostructure. The developed material system and demonstrated memory device fabrication can be significant for next generation data storage applications. © *2014 AIP Publishing LLC*. [http://dx.doi.org/10.1063/1.4903552]

I. INTRODUCTION

Significant interest has been given to two dimensional (2D) materials after the discovery of graphene, considering the fascinating electronic properties for novel device applications.[1–4] Besides graphene related materials, quasi-two-dimensional transition metal dichalcogenides (TMDCs) are gaining lot of attention due to presence of a band gap for practical electronic device applications.[5–8] Among various TMDCs, molybdenum disulfide (MoS_2) is of great interest for next generation field effect transistors (FETs) and optoelectronic devices owing to presence of a direct band gap ($\sim$1.85 eV) in monolayer; whereas an indirect band gap ($\sim$1.29 eV) is observed in bulk state.[5,9–11] Fabrication of FETs, sensors, phototransistors, and energy storage devices have been demonstrated using monolayer and few-layer MoS_2.[11–17] Excellent on/off ratio ($\sim 10^8$) in a FET device with high carrier mobility has been obtained due the presence of direct band gap, whereas on/off ratio is significantly poor in sp^2 hybridized graphene.[12] Recently, heterojunction of graphene and MoS_2 has been significantly explored to take the advantage of metallic and semiconducting properties of the respective materials.[18,19] Multifunctional photoresponsive memory device has been demonstrated with a graphene-MoS_2 hybridized structure.[20] Again, non-volatile memory device based on FET device has been fabricated with graphene, hexagonal boron nitride, and MoS_2 stacked 2D materials.[21,22]

Considering the rapid development of 2D materials for next generation device applications, several methods have been explored to derive or synthesized MoS_2 layers.[5,11,23–28] There have been efforts to produce monolayer and few-layer MoS_2 by micromechanical exfoliation process.[5,11] MoS_2 layers were also derived with intercalation-assisted and solution-based chemical exfoliation process.[23,24] On the other hand, hydrothermal method, physical vapor deposition, electrochemical synthesis, and chemical vapor deposition (CVD) techniques were developed to synthesize MoS_2 sheets.[25,26] Similarly, large-area uniform growth of MoS_2 layer has been achieved by sulfurization of Mo and molybdenum oxide (MoO_3).[27,28] In the sulfurization process, assembling the atoms on an arbitrary substrate to obtain a controlled or patterned MoS_2 structure in a large-area can be most significant. Controlled synthesis of MoS_2 crystals in large-area is one of the important aspects for its integration in photovoltaic, phototransistors, and memory device applications. In contrast to previous reports, we demonstrate synthesis of elongated hexagonal and rhombus shaped MoS_2 crystals by sulfurization of MoO_3 thin film and fabrication of poly(methyl methacrylate) (PMMA)-MoS_2/graphene heterostructure memory device. In the fabricated device, PMMA layer plays a dual role of supporting layer for transfer process and as an insulating dielectric in the memory device. The developed material system and observation of bistable electrical switching effect can be significant for development of future generation of non-volatile memory devices.

II. EXPERIMENTAL

In this study, MoO_3 (purity $\sim$ 99.0%) and S (purity $\sim$ 98.0%) powder purchased from Wako chemicals were used for synthesis of MoS_2 crystals. MoO_3 thin film with optimized thickness was deposited on a SiO_2/Si

a)Author to whom correspondence should be addressed. Electronic mail: kalita.golap@nitech.ac.jp. Tel./Fax: +81-52-735-5216.

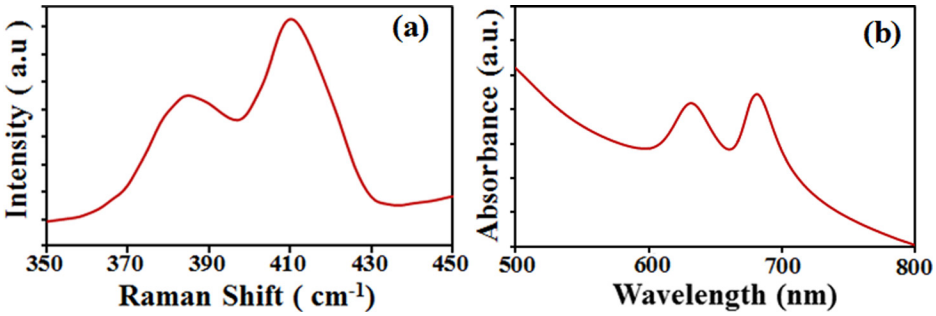

FIG. 1. (a) Raman spectra of as-synthesized MoS_2 crystals by sulfur reaction process of thermally evaporated MoO_3 thin film. (b) UV-visible spectra of the transferred MoS_2.

substrate by thermal evaporation. The MoO_3 thin film coated on SiO_2/Si substrate was placed in a CVD furnace under the flow of 80 sccm Ar and 20 sccm H_2 mixture, whereas S powder was kept at room temperature zone. When the hot zone reached to desired temperature (~650 °C), S powder was evaporated at 300 °C. Subsequently, the furnace heater was turned off after finishing the S powder evaporation, and the sample was left in the chamber to cool down. Graphene film synthesized on Cu foil by an atmospheric pressure CVD was used for device fabrication and transferred onto a SiO_2/Si substrate. Synthesized MoS_2 film was coated with PMMA solution of 1 mg/ml in acetone, as the supporting layer for the transfer process. Etching of the PMMA coated MoS_2 layer from SiO_2/Si substrate was achieved with an 11 M NaOH solution at 100 °C. A memory device was configured with the PMMA-MoS_2 transferred layer on graphene film. A top gold electrode (~25 nm) was deposited on PMMA-MoS_2 layer to complete the device structure. Synthesized MoS_2 crystals were characterized by Raman and UV-visible absorption spectroscopy. Raman studies of MoS_2 crystals and graphene film were carried out with NRS 3300 laser Raman spectrometer with a laser excitation energy of 532.08 nm. UV-visible absorption spectroscopy was carried out with JASCO V-670 K spectrophotometer. Transmission electron microscope (TEM) images were taken by JEOL JEM 2100, operated at 200 kV equipped with an element analyzer. Scanning transmission electron microscope (STEM) studies of MoS_2 crystals were carried out by JEM-ARM 200F. Optical microscopy studies of graphene and fabricated heterostructure were carried out with VHX-500 digital microscope. Scanning electron microscope (SEM) study was carried out with Hitachi S-4300 operated at an acceleration voltage 20 kV. The MoO_3 film and Au electrode were deposited by thermal evaporation technique using ULVAC VPC-260F. Current-voltage (I-V) characteristic measurements were carried out using two probe system and Keithley 2401 Source Meter.

III. RESULTS AND DISCUSSION

Figure 1(a) shows Raman spectra of as-synthesized MoS_2 layer by the sulfur reaction process of MoO_3 thin film. Two characteristic peaks at 409.8 and 385.6 cm^{-1} are observed corresponding to A_{1g} mode associated with out of plane vibration of sulfur atoms and E_{2g} mode related with in-plane vibration of Mo and sulfur atoms. Broadening of the Raman peaks is considered to be due to phonon confinement, as well as signifying smaller lateral size of the synthesized MoS_2 crystals. Again, the frequency difference between the A_{1g} and E_{2g} modes is found to be 24.2 cm^{-1}, corresponding to growth of few-layer structure. While, the frequency difference has been found to be around 20.4 cm^{-1} for a CVD synthesized monolayer MoS_2.[29] Figure 1(b) shows UV-visible spectra of the transferred MoS_2 film on glass substrate. Two prominent absorption peaks are observed at 628 and 680 nm corresponding to direct excitonic transitions. It has been reported that the peak positions of the absorption spectra corresponding to the direct excitonic states can varies with change in number of layers.[8] For monolayer and few-layer MoS_2, the two exciton peaks show blue-shift due to quantum confinement effect as the thickness of the crystal decrease.[30]

The crystallinity and structural morphologies of the synthesized MoS_2 crystals were investigated by TEM studies. Figures 2(a) and 2(b) show TEM bright-field images of as-synthesized MoS_2, presenting elongated-hexagonal and rhomboidal shape of the crystals. Previously, rhomboidal shaped MoS_2 flakes has been grown using a MoO_2 microcrystals as template; however, formation of elongated-hexagonal flakes were not observed.[31] The shape of a crystal is determined by the growth rate of different crystal faces. In

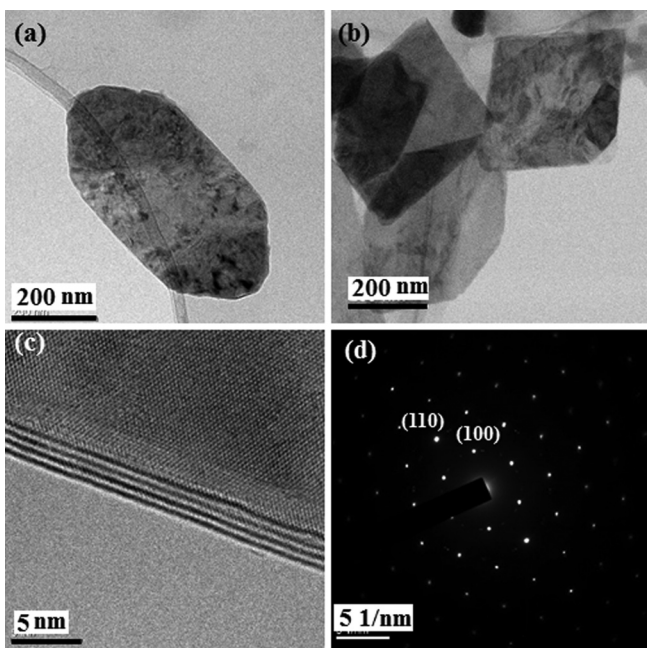

FIG. 2. TEM bright-field images of synthesized MoS_2, presenting (a) elongated-hexagonal and (b) rhomboidal shapes. (c) Few-layer structure with a layer spacing of about ~0.65 nm. (d) SAED pattern taken from the MoS_2 crystal, presenting the hexagonal symmetric structure.

this prospect, the slowest growing face become largest, whereas faster growing face can become smaller or disappear. In a CVD process, the shape of MoS_2 crystals can change depending on the Mo:S ratio, substrate position and flow direction significantly influencing the growth kinetic of edges.[32] Figure 2(c) shows layer numbers of a hexagonal flake as obtained at the folded edge. The MoS_2 crystal with four layers shows a layer spacing of about 0.65 nm. Figure 2(d) shows selected area electron diffraction (SAED) pattern taken from the MoS_2 crystal, presenting the hexagonal symmetric structure. The SAED pattern also shows the (100) and (110) lattice planes of the MoS_2 crystals. Recently, large-area MoS_2 thin layer has been synthesized by two step thermal reduction and sulfurization process of MoO_3 thin film.[33] In contrast to previous finding, we demonstrate synthesis of hexagonal and rhombus shaped MoS_2 crystals with a sulfurization process of MoO_3 thin film.

The structural morphology was further analyzed with aberration corrected STEM high-angle annular dark-field (HAADF), also known as Z-contrast imaging. At the edge of a MoS_2 crystal, we can observe the atomic structure of a single layer as shown in Figure 3(a). The Mo and S atoms can be directly identified from the contrast of the image, signifying highly ordered and crystalline MoS_2 layer. Figure 3(b) shows a Fourier-filtered image corresponding to the HAADF image, presenting better view of the lattice structure of the MoS_2 layer. The Mo atoms show higher contrast than that of S atoms. In the inset of figure, we present the atomic arrangement of Mo and S atoms to form a MoS_2 layer. Figure 3(c) shows cross-section HAADF image of the synthesized few-layer MoS_2 crystal, presenting high quality lattice structure. Figure 3(d) shows the corresponding Fourier-filtered image of the cross-section HAADF image, where direct evaluation of the lattice constant is possible. Inset of the figure shows line profile across the filtered image as marked in Figure 3(d). A lattice constant around ~0.312 nm is estimated from the line profile for the MoS_2 crystal.

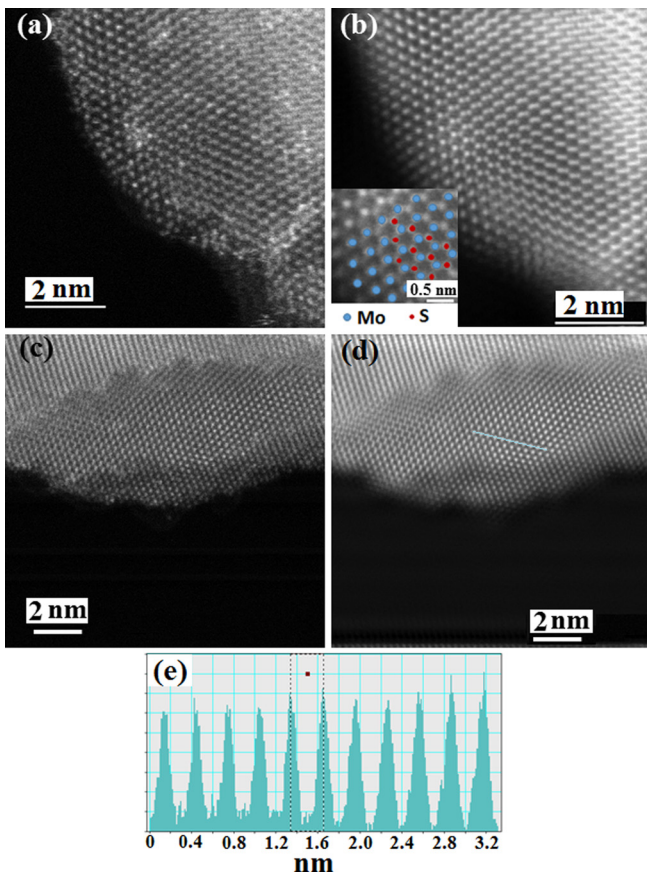

FIG. 3. (a) HAADF image of a MoS_2 crystal at the edge. (b) Fourier-filtered image corresponding to the HAADF image, presenting better view of the lattice structure. In the inset of figure, atomic arrangement of Mo and S atoms to form a MoS_2 layer is presented. (c) Cross-section HAADF image of few-layer MoS_2 crystal. (d) Corresponding Fourier-filtered image of the cross-section HAADF image. (e) Line profile across the filtered image as marked in Figure 3(d).

Figure 4(a) shows transfer process of the synthesized graphene and MoS_2 crystals for the fabrication of heterojunction memory device. High quality graphene synthesized on Cu foil by the solid precursor based CVD process was transferred onto a SiO_2/Si substrate. Figure 4(b) shows an optical image at the edge of the transferred graphene film. From the color contrast, the graphene film can be directly identified on the SiO_2/Si substrate. Figure 4(c) shows Raman spectra of the graphene film. Graphitic G and second order 2D Raman peaks are observed at 1589 and 2700 cm^{-1}, respectively. The ratio of G to 2D peak intensity (I_G/I_{2D}) is found to be around 1.3, signifying presence of more than single layer graphene. The synthesized MoS_2 crystals coated with PMMA solution was then transferred on the high quality graphene. Figure 4(d) shows an optical microscope image of the transferred PMMA-MoS_2 on graphene film. The layer-by-layer transferred PMMA-MoS_2 on graphene can form a close contact hybridized heterostructure with strong van der Waals interaction. Figure 4(e) shows a top-view SEM image of the PMMA-MoS_2 hybrid structure. PMMA coating can hold MoS_2 crystals together and at the same time act as the dielectric interface for memory device. The dual role of PMMA in the MoS_2 crystals and CVD graphene based memory device has not been explored. Hence, it is an interesting aspect of the developed material system, which can be integrated for the memory device application.

Figure 5(a) shows a schematic diagram of the fabricated PMMA-MoS_2/graphene heterostructure as a memory device. In the fabricated device, PMMA-MoS_2 hybrid structure is the functional material, whereas the continuous CVD graphene film acts as the electrode. Figure 5(b) shows a typical I–V characteristic of the PMMA-MoS_2/graphene heterojunction device. Increasing the applied potential (V) from 0 to 5 V, the current increases gradually (stage I), while an abrupt increase in current occurred from 0.052 mA to 0.127 mA (stage II). This indicates transition of the device from a high resistance state (HRS) to low resistance state (LRS). The fabricated heterojunction shows good stability in the LRS during the subsequent voltage sweep in stages III and IV, signifying the nonvolatile memory effect. Repeated measurements also show identical device characteristics in the developed heterostructure material system. A device fabricated with higher amount of PMMA solution casted on the MoS_2 crystals shows much higher on/off ratio as shown in Figure 5(c). Abrupt increase in current is observed from stage I to stage II with an on/off ratio as high as 2.5×10^3.

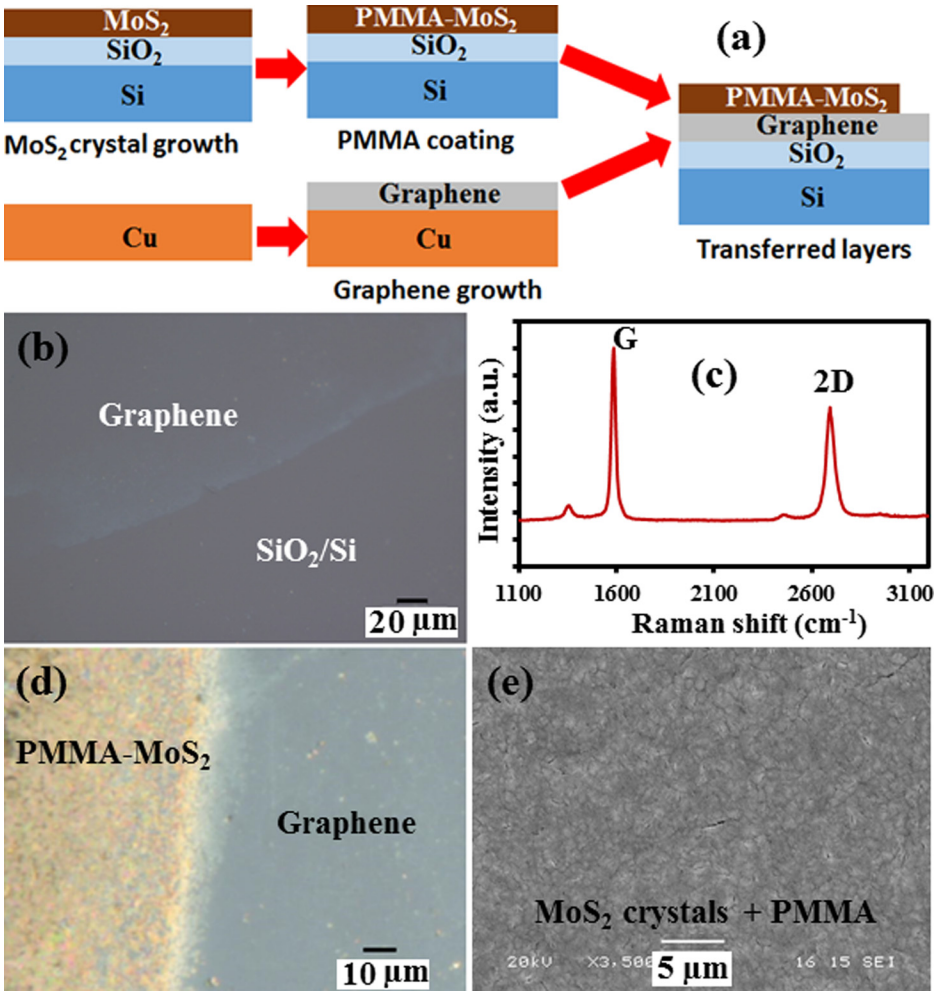

FIG. 4. (a) Transfer process of the synthesized graphene and MoS_2 crystals for the fabrication of heterojunction memory device. (b) Optical microscope image and (c) Raman spectra of the transferred graphene. (d) Optical microscope image of the transferred PMMA-MoS_2 on graphene film. (e) Top view SEM image of the PMMA-MoS_2 hybrid structure.

The memory characteristic of the fabricated device can be attributed to charge trapping and detrapping behavior of MoS_2 in presence of PMMA. The lowest unoccupied molecular orbital (LUMO) and highest occupied molecular orbital (HOMO) levels of PMMA are around −1.8 eV and −7.3 eV, respectively, with an energy gap of ∼5.5 eV.[34] Again, Few-layer MoS_2 have low electron affinities of around ∼3.0 eV, with a band gap in the range of 1.4–1.8 eV. Hence, it will create a large electron and hole injection barrier with an applied potential. Charge transfer occurs between the

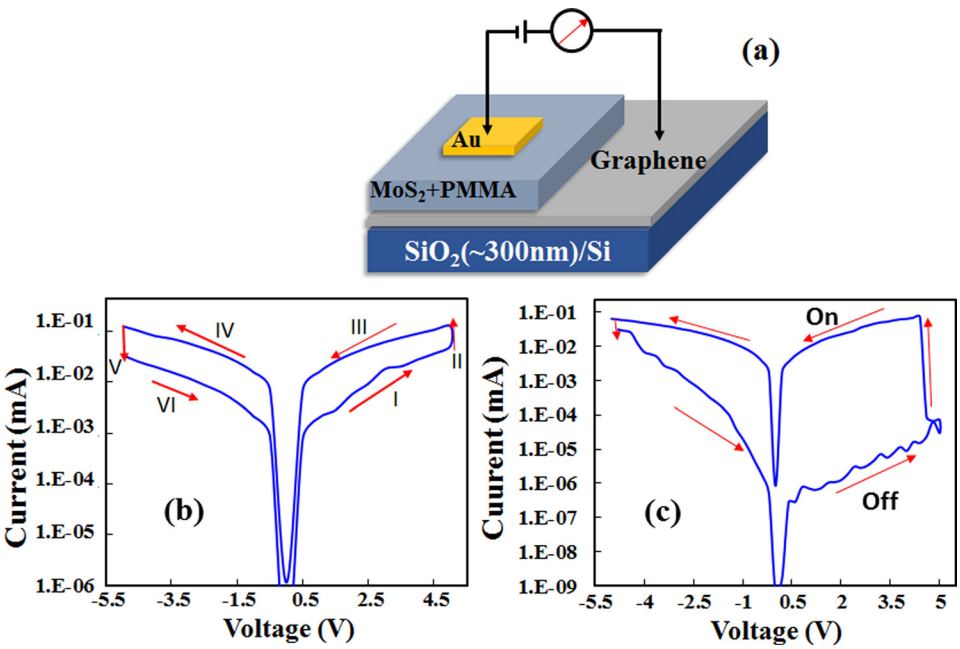

FIG. 5. (a) Schematic diagram of the fabricated PMMA-MoS_2/graphene heterostructure as a memory device. (b) and (c) Typical I-V characteristic of the PMMA-MoS_2/graphene heterojunction device varying the amount of PMMA solution coated on MoS_2 film.

PMMA and MoS_2 crystals in the hybridized structure, subsequently trapping of charge in MoS_2 due to its lower energy level and quantum confinement effect. In the demonstrated device, top electrode and PMMA-MoS_2 functional material composition is still unoptimized, which provide ample opportunity for fabrication of an efficient memory device. This nonvolatile rewritable feature of the fabricated PMMA-MoS_2/graphene heterojunction device can be used as electrically bistable material in the flash memory device. The demonstrated MoS_2 crystal synthesis process and their integration to fabricate heterojunction memory device can be significant prospect for memory device applications.

IV. CONCLUSION

In summary, we have demonstrated the synthesis of elongated hexagonal and rhombus shaped MoS_2 crystals by sulfurization of thermally evaporated MoO_3 thin film. TEM and STEM-HAADF studies were performed to reveal the atomic level structure of the synthesized high quality MoS_2 crystals. A hybridized structure of graphene and MoS_2 was fabricated with layer-by-layer transfer process to configure a memory device. The PMMA layer used for transfer process of MoS_2 film performed a dual role of supporting and insulting dielectric layer in the fabricated memory device. The memory device was configured with PMMA-MoS_2 and CVD graphene as functional and electrode materials, respectively. Typical bistable electrical switching and nonvolatile rewritable memory effect was observed in the fabricated PMMA-MoS_2/graphene heterostructure. An on/off ratio as high as 2.5×10^3 was obtained in the fabricated PMMA-MoS_2/graphene memory device. The memory characteristic of the fabricated device is attributed to the charge trapping and detrapping behavior of MoS_2 in presence of PMMA. The developed material system and demonstrated memory device fabrication process can be significant platform for next generation data storage applications.

ACKNOWLEDGMENTS

This work was supported by the funds for the development of human resources in science and technology, Japan.

[1]A. K. Geim and K. S. Novoselov, Nat. Mater. **6**, 183 (2007).
[2]K. I. Bolotin, F. Ghahari, M. D. Shulman, H. L. Stormer, and P. Kim, Nature **462**, 196 (2009).
[3]Y. Lin, A. Valdes-Garcia, S. Han, D. Farmer, I. Meric, Y. Sun, Y. Wu, C. Dimitrakopoulos, A. Grill, P. Avouris, and K. Jenkims, Science **332**, 1294 (2011).
[4]C. Zhi, Y. Bando, C. Tang, H. Kuwahara, and D. Olberg, Adv. Mater. **21**, 2889 (2009).
[5]K. F. Mak, C. Lee, J. Hone, J. Shan, and T. F. Heinz, Phys. Rev. Lett. **105**, 136805 (2010).
[6]N. Coleman, M. Lotya, A. O'Neill, S. Bergin, P. King, U. Khan, K. Young, A. Gaucher, S. De, and R. Smith, Science **331**, 568 (2011).
[7]B. Radisavljevic, A. Radenovic, J. Brivio, V. Giacometti, and A. Kis, ACS Nano **5**, 9934 (2011).
[8]A. Splendiani, L. Sun, Y. Zhang, T. Li, J. Kim, C. Y. Chim, G. Galli, and F. Wang, Nano Lett. **10**, 1271 (2010).
[9]M. Shanmugam, C. A. Durcan, and B. Yu, Nanoscale **4**, 7399 (2012).
[10]H. Liu and P. D. Ye, IEEE Electron Device Lett. **33**, 546 (2012).
[11]B. Radisavljevic, A. Radenovic, J. Brivio, V. Giacometti, and A. Kis, Nat. Nanotechnol. **6**, 147 (2011).
[12]Y. Zhang, J. Ye, Y. Matsuhashi, and Y. Iwasa, Nano Lett. **12**, 1136 (2012).
[13]Y. Cai, G. Zhang, and Y. W. Zhang, J. Am. Chem. Soc. **136**, 6269 (2014).
[14]H. Li, Z. Yin, Q. He, H. Li, X. Huang, G. Lu, D. W. H. Fam, A. Y. Tok, Q. Zhang, and H. Zhang, Small **8**, 63 (2012).
[15]Z. Y. Yin, H. Li, H. Li, L. Jiang, Y. M. Shi, Y. H. Sun, G. Lu, Q. Zhang, X. D. Chen, and H. Zhang, ACS Nano **6**, 74 (2012).
[16]J. Xiao, D. Choi, L. Cosimbescu, P. Koech, J. Liu, and J. P. Lemmon, Chem. Mater. **22**, 4522 (2010).
[17]H. S. Lee, S. W. Min, Y. G. Chang, M. K. Park, T. Nam, H. Kim, J. H. Kim, S. Ryu, and S. Im, Nano Lett. **12**, 3695 (2012).
[18]A. K. Geim and I. V. Grigorieva, Nature **499**, 419 (2013).
[19]H. J. Chuang, X. Tan, N. J. Ghimire, M. M. Perera, B. Chamlagain, M. M. C. Cheng, J. Yan, D. Mandrus, D. Tománek, and Z. Zhou, Nano Lett. **14**, 3594 (2014).
[20]K. Roy, M. Padmanabhan, S. Goswami, T. P. Sai, G. Ramalingam, S. Raghavan, and A. Ghosh, Nat. Nanotechnol. **8**, 826 (2013).
[21]S. Bertolazzi, D. Krasnozhon, and A. Kis, ACS Nano **7**, 3246 (2013).
[22]M. S. Choi, G. H. Lee, Y. J. Yu, D. Y. Lee, S. H. Lee, P. Kim, J. Hone, and W. J. Yoo, Nat. Commun. **4**, 1624 (2013).
[23]K. G. Zhou, N. N. Mao, H. X. Wang, Y. Peng, and H. L. Zhang, Angew. Chem. Int. Ed. **50**, 10839 (2011).
[24]H. S. S. M. Ramakrishna, A. Gomathi, A. K. Manna, D. J. Late, R. Datta, S. K. Patil, and C. N. R. Rao, Angew. Chem. Int. Ed. **49**, 4059 (2010).
[25]S. Helveg, J. V. Lauritsen, E. Lægsgaard, I. Stensgaard, J. K. Nørskov, B. S. Clausen, H. Topse, and F. Besenbacher, Phys. Rev. Lett. **84**, 951 (2000).
[26]Y. H. Lee, X. Q. Zhang, W. Zhang, M. T. Chang, C. T. Lin, K. D. Chang, Y. C. Yu, J. T. W. Wang, C. S. Chang, L. J. Li, and T. W. Lin, Adv. Mater. **24**, 2320 (2012).
[27]H. Hadouda, J. Pouzet, J. C. Bernede, and A. Barreau, Mater. Chem. Phys. **42**, 291 (1995).
[28]S. Balendhran, J. Z. Ou, M. Bhaskaran, S. Sriram, Z. Ippolito, E. Kats, S. Bhargava, S. Zhuiykov, and K. Kalantar-zadeh, Nanoscale **4**, 461 (2012).
[29]Y. Yu, C. Li, Y. Liu, L. Su, Y. Zhang, and L. Cao, Sci. Rep. **3**, 1866 (2013).
[30]H. Shi, R. Yan, S. Bertolazzi, J. Brivio, B. Gao, A. Kis, S. Jena, H. G. Xing, and L. Huang, ACS Nano **7**, 1072 (2013).
[31]X. Wang, H. Feng, Y. Wu, and L. Jiao, J. Am. Chem. Soc. **135**, 5304 (2013).
[32]S. Wang, Y. Rong, Y. Fan, M. Pacios, H. Bhaskaran, K. He, and J. H. Warner, Chem. Mater. **26**, 6371 (2014).
[33]Y. C. Lin, W. Zhang, J. K. Huang, K. K. Liu, Y. H. Lee, C. T. Liang, C. W. Chu, and L. J. Li, Nanoscale **4**, 6637 (2012).
[34]Y. J. Yun, C. Pearson, and M. C. Petty, J. Appl. Phys. **105**, 034508 (2009).